Fuel 326 (2022) 124966

Contents lists available at ScienceDirect

Fuel

journal homepage: www.elsevier.com/locate/fuel

Full Length Article

Combined effect of bio-oil composition and temperature on the stability of Ni spinel derived catalyst for hydrogen production by steam reforming

Naiara García-Gómez, José Valecillos *, Beatriz Valle, Aingeru Remiro, Javier Bilbao, Ana G. Gayubo

Department of Chemical Engineering, University of the Basque Country (UPV/EHU) P.O. Box 644, Bilbao 48080 Spain

ARTICLE INFO

Keywords:
Bio-oil steam reforming
Hydrogen
$NiAl_2O_4$ spinel
Catalyst deactivation
Coke deposition

ABSTRACT

A challenge for scaling up hydrogen production by raw bio-oil steam reforming (SR) is the rapid catalyst deactivation that is strongly sensitive to the temperature and bio-oil composition. This work studies the combined effect of both variables on the stability of a Ni/Al_2O_3 catalyst with high Ni dispersion in the internal and external surfaces of the particles, obtained by reduction of a $NiAl_2O_4$. The raw bio-oil composition is modified by (i) removal of phenolic compounds by liquid–liquid extraction or (ii) use of an online pre-reforming step with dolomite. Then, SR tests of the bio-oils at 600 and 700 °C are carried out in a system with two online units, the first one for controlled deposition of pyrolytic lignin (and also pre-reforming with dolomite) and the second one (fluidized bed reactor) for the SR of the volatile oxygenates. The time on stream evolution of the conversion and products yields is related to the amount, nature and location of coke in the catalyst particles, determined with several techniques. For bio-oils with high or moderate phenolic content (raw or pre-reformed bio-oil, respectively), the SR at 600 °C leads to a moderate deactivation. However, at 700 °C, a refractory coke is formed, mainly composed of carbon filaments and turbostratic carbon among them that causes a rapid catalyst deactivation by blocking the external surface of the catalyst particle. Conversely, the removal of phenolic compounds from raw bio-oil leads to a more stable SR operation at 700 °C, because the formation of turbostratic carbon is slowed down.

1. Introduction

The depletion of fossil fuels, the implementation of stricter environmental policies aimed at mitigating net CO_2 emissions and the social environmental awareness have attracted increasing attention on energy production from renewable sources [1]. Hydrogen (H_2) plays a key role as an energy vector in this crucial transition from fossil fuels based economy towards a decarbonized economy [2]. Particularly, sustainable production of H_2 from lignocellulosic biomass (which does not interfere with human and animal food chains) and its derivatives is of interest [3–5] because it is a complementary strategy to H_2O electrolysis, that can be integrated into energy and economic policies to improve the forestry and agricultural waste management, with a neutral CO_2 balance. Among the H_2 production routes from biomass, the steam reforming (SR) of bio-oil is a promising and economically viable technology that has gained increased attention [6–8]. Bio-oil can be produced in delocalized way, by means of well-developed fast pyrolysis technologies in simple equipment and with low operating costs [9]. Likewise, bio-oil has a higher energy density and is easier to transport than biomass, which allows its reforming to be centralized in a facility (bio-refinery) with units designed *ad-hoc* for the selective production of H_2 [10]. In addition, the SR of bio-oil to produce H_2 avoids the costly water separation process required by other bio-oil upgrading technologies [11,12].

The overall stoichiometry of SR of oxygenates in bio-oil, Eq. (1), is a combination of the stoichiometry for producing CO and H_2 (Eq. (2)) and that of subsequent water gas shift (WGS) reaction (Eq. (3)):

$$C_nH_mO_k + (2n - k)H_2O \rightarrow nCO_2 + (2n + m/2 - k)H_2 \quad (1)$$

$$C_nH_mO_k + (n - k)H_2O \rightarrow nCO + (n + m/2 - k)H_2 \quad (2)$$

$$CO + H_2O \leftrightarrow CO_2 + H_2 \quad (3)$$

Nevertheless, other secondary reactions take place, such as decomposition/cracking (Eq. (4)), reforming of CH_4 and hydrocarbons formed

* Corresponding author.
E-mail address: jose.valecillos@ehu.eus (J. Valecillos).

https://doi.org/10.1016/j.fuel.2022.124966
Received 4 April 2022; Received in revised form 16 June 2022; Accepted 17 June 2022
Available online 28 June 2022

by decomposition (Eqs. (5) and (6), respectively), decomposition of CH_4 and hydrocarbons (Eqs. (7) and (8), respectively), Boudouard reaction (Eq. (9)) and carbon gasification reaction (Eq. (10)). These reactions reduce the H_2 yield and originate gaseous carbon by-products as well as carbonaceous deposits (coke) that deactivate the catalyst. Minimizing catalyst deactivation, with coke deposition as the main cause, is one of the main challenges to overcome for the large-scale development of bio-oil SR.

$$C_nH_mO_k \rightarrow C_xH_yO_z + C_rH_s + CH_4 + H_2O + CO + CO_2 + H_2 + C(coke) \quad (4)$$

$$CH_4 + H_2O \leftrightarrow CO + 3H_2 \quad (5)$$

$$C_aH_b + aH_2O \leftrightarrow aCO + (a + b/2)H_2 \quad (6)$$

$$CH_4 \leftrightarrow 2H_2 + C(coke) \quad (7)$$

$$C_aH_b \rightarrow (b/2)H_2 + aC(coke) \quad (8)$$

$$2CO \leftrightarrow CO_2 + C(Coke) \quad (9)$$

$$C(coke) + H_2O \rightarrow CO + H_2 \quad (10)$$

The structure and composition of the catalyst, the operating conditions and the bio-oil composition are the three main factors that determine the H_2 yield and the stability of the catalyst in the bio-oil SR. The most common catalysts used are based on Ni supported on different materials without or with promoters/additives and prepared by different methods [11,13]. Ni is the preferred active phase because its capacity to break C–C bonds, absorb and dissociate water and for its low cost. Among different catalytic systems studied for the SR of bio-oil feeds, those obtained from the reduction of Ni/Al spinel structures prepared by coprecipitation are a promising alternative [14–19] because it allows to incorporate large Ni loadings with a good dispersion, thus promoting the SR of oxygenates in the bio-oil. The preparation of this catalyst is simple and reproducible consisting of obtaining the $NiAl_2O_4$ spinel structure by coprecipitation and calcination at high temperature [16,19,20], and subsequent reduction with H_2, that causes the exsolution of Ni and transforms the spinel phase into reduced Ni crystals and Al_2O_3 phases. The resulting Ni/Al_2O_3 catalyst consist of highly dispersed reduced Ni crystals that are homogeneously located over all the particle internal and external surfaces. Likewise, the modification of Ni catalysts with Ce, Co, Cu or Mg could enhance the H_2 yield and catalyst stability under different conditions and reactors [14,21,22].

The selection of operating conditions affects both the extent of the reactions involved in the SR of bio-oil [23–25] and the stability of the catalyst [19,26–30]. The increase in the space time (or decrease in the space velocity) has a favorable effect because it increases the oxygenates conversion through SR (Eq. (2)) and WGS (Eq. (3)) reactions and enhances the catalyst stability due to lower coke formation by oxygenates decomposition (Eq. (4)), thus leading to a higher and more stable H_2 production [19,26,29,31].

The effect of temperature is more complex, since it has a counteracting effect both on the extent of H_2 formation reactions and on the causes of deactivation (coke deposition and sintering). On one hand, the increase in temperature promotes the SR reactions of oxygenates (Eq. (2) and their decomposition products (Eqs. (5) and (6)), but disfavors the WGS reaction (Eq. (3)) [19,25,32]. On the other hand, increasing the temperature attenuates the CO disproportionation (Boudouard) reaction (Eq. (9)) and promotes coke gasification (Eq. (10)) [33,34] but favors coke formation reactions by cracking/decomposition of oxygenates (Eq. (4)) and decomposition of CH_4 and hydrocarbons (Eqs. (7) and (8), respectively), [27,35] and also can promote metallic sintering [32,36]. To achieve high H_2 conversion and yield, higher operating temperatures (usually 800 or 900 °C) are required for SR of high phenolic feeds [27,37] than for SR of light oxygenates, such as acetic acid. Thus, Kumar and Sinha found an optimum temperature of 600 °C for the SR of acetic acid over $Ni/\gamma\text{-}Al_2O_3\text{-}La_2O_3\text{-}CeO_2$ [38].

Concerning steam to carbon (S/C) ratio in the feed, its increase favors the extent of SR and WGS reactions [32,39–41] and also coke gasification reactions at high temperatures [29,32,42], but excess of water could decrease the catalytic activity due to competitive adsorption on active sites [26,27,43–45] and also causes irreversible deactivation by sintering phenomenon when operating at high temperatures [36].

The effect of the bio-oil composition can be understood compiling several studies of SR with pure oxygenates [46–50], as well as with bio-oil aqueous fractions [51] or raw bio-oil [52,53], that have shown the different role of the different families of oxygenates in the bio-oil on the catalyst kinetic behavior (activity and stability). Remon et al. [51] reported that the concentration of acetic acid and furfural had the greatest impact on the reforming results for different aqueous fractions of bio-oil at 650 °C over a Ni-Co/Al-Mg catalyst: acetic acid showed low reactivity but produced low coke formation, whereas furfural had high reactivity and high tendency to produce coke. It should be noted that the characteristics (structure, morphology and location) of the coke deposits have a greater impact on catalyst deactivation than the amount of coke deposited [54], with these characteristics being highly dependent on the functionality of the oxygenated compounds reformed. Wang et al. [55] observed a slightly faster deactivation of a Ni/SBA-15 catalyst in the SR at 650 °C of carboxylic acid than of alcohols, in spite of the lower amount of coke deposited. The authors attributed these results to the formation of more amorphous and encapsulating coke in the SR of the carboxylic acids due to their higher tendency towards cracking/decomposition. Ochoa et al. [56] highlighted the relevant role of phenolic compounds as the main precursors of amorphous and encapsulating coke deposition, which caused the rapid deactivation of the $Ni/La_2O_3\text{-}\alpha Al_2O_3$ catalyst in the SR of raw bio-oil at 550 °C.

Likewise, bio-oil has heavy components that polymerize at the reactor inlet forming pyrolytic lignin (PL), which causes a rapid catalyst deactivation. It has been proven that the controlled deposition of PL in a raw bio-oil thermal treatment unit (at 500 °C) is effective in mitigating catalyst deactivation in the online reforming reactor [29,57,58]. However, catalyst deactivation is also noticeable under these conditions.

The adverse effect of some compounds present in the raw bio-oil motivates the modification of its composition with the purpose of enhancing the catalyst stability. Accordingly, one strategy is the removal of phenolic compounds. Valle et al. [52], demonstrated the efficacy of this strategy (by liquid–liquid (L-L) solvent-anti-solvent extraction with dichloromethane and water) to attenuate the deactivation of the $NiAl_2O_4$ spinel derived catalyst in SR at 700 °C. Another strategy studied by Garcia-Gómez et al. [53] is the use of a previous pre-reforming step with dolomite that affects the stability of the main reforming catalyst (derived from $NiAl_2O_4$ spinel) in the subsequent SR of the oxygenates stream at 700 °C. It is remarkable the different effect depending of pre-reforming temperature: at low temperature (400 °C) the concentration of acids, phenols and saccharides (mainly levoglucosan) decreased, and that of ketones increased, which improved the stability of the Ni catalyst due to a lower deposition of graphitic coke. Conversely, the pre-reforming at 700 °C boosted the formation of phenols and hydrocarbons in the oxygenates stream, to the expense of ketones and acids, which promoted the deposition of amorphous and encapsulating coke on the Ni catalyst that caused a faster deactivation.

In this work, we have investigated the combined effect of reforming temperature and bio-oil composition on the stability of a Ni/Al_2O_3 catalyst obtained upon reduction (4 h at 850 °C) of a $NiAl_2O_4$ spinel. This catalyst has good perspectives for use in the bio-oil SR to an industrial scale due to its high activity and H_2 selectivity [16,18,19] and, more importantly, because has reproducible performance in successive reaction-regeneration-reduction cycles [17,59]. In our previous work [19], we have found that the reaction conditions (in particular the temperature) have a significant effect on the coke nature and location on this catalyst: above 600 °C, the fast coke deposition on the external

surface leads to a lower stability than in the SR at 600 °C. But it should be noted that the use of bio-oil treatments prior to the reforming reaction (such as phenols extraction or pre-reforming with dolomite) significantly affects the bio-oil composition, which could affect the prevailing mechanisms of coke formation at different temperatures. We have studied the SR at low (600 °C) and high (700 °C) temperature of three bio-oils with significant differences in their composition: i) raw bio-oil (denoted RB); ii) bio-oil treated by L-L extraction to remove phenolic compounds (denoted TB); iii) and bio-oil subject to an on-line pre-reforming step with dolomite, prior to the SR with the Ni catalyst (denoted PRB). The coke deposited on the used catalyst after each reforming reaction was characterized with several techniques (X-ray diffraction (XRD), temperature programed oxidation (TPO), Raman spectroscopy and scanning electron microscopy (SEM) images) in order to analyze its amount, structure, morphology and location, and relate it to the catalyst stability. The results show the interest of the previous separation of phenolic compounds in the bio-oil and of the operation at 700 °C to avoid the rapid deactivation of the catalyst.

2. Experimental

2.1. Catalysts preparation and characterization

The $NiAl_2O_4$ spinel (with 33 wt% Ni) was synthetized by the co-precipitation method [18,60]. The precipitating agent (0.6 M solution of NH_4OH) was added dropwise to an aqueous solution of Ni $(NO_3)_2{\cdot}6H_2O$ (Panreac, 99%) and $Al(NO_3)_3{\cdot}9H_2O$ (Panreac, 98%) at 25 °C until reaching a pH of 8. After homogenizing for 30 min, the precipitate was recovered by filtration, washed with distilled water to remove the remaining ammonium ions, dried at 110 °C overnight, calcined at 850 °C for 4 h with a heating ramp of 10 °C min^{-1}, and crushed and sieved to obtain particle sizes in the range of 0.15–0.25 mm.

The $NiAl_2O_4$ spinel structure was characterized by temperature-programmed reduction (TPR), and X-ray diffraction (XRD). The TPR analysis (in a Micromeritics AutoChem II 2920) was carried out under a H_2(10 % vol)/Ar flow from 50 °C up to 950 °C with a heating ramp of 5 °C min^{-1}.The TPR profile (Fig. S1 in Supplementary Material) showed a sole reduction peak between 600 and 800 °C, with a maximum hydrogen uptake at ~ 770 °C, corresponding to the reduction of Ni^{2+} species in a $NiAl_2O_4$ spinel structure [17]. The XRD analysis of the reduced catalyst was carried out in a Bruker D8 Advance diffractometer equipped with a Germanium primary monochromator, Bragg-Brentano geometry and with a CuKα1 wavelength of 1.5406 Å, and with data collection from 10° to 80° with step of 0.04° in 2θ. The XRD diffractogram confirmed the sole presence of Al_2O_3 and Ni^0 particles, and allowed calculating the average size of Ni^0 crystals by means of the Scherrer equation (applied to the diffraction peak at the (200) plane (2θ = 51.8°).

The Ni catalyst used in each reaction was analyzed by XRD, temperature programmed oxidation (TPO), Raman spectrocopy and scanning electron microscopy (SEM) images. The TPO analyses were carried out in a Thermo Scientific TGA Q5000TA IR thermobalance coupled in line with a Thermostar Balzers Instrument mass spectrometer for monitoring CO_2 signal, because the oxidation of Ni particles during combustion masks the thermogravimetric signal. The procedure consisted of stabilizing the sample at 50 °C, followed by heating up to 800 °C under 50 cm^3 min^{-1} airflow with a heating ramp of 5 °C min^{-1}. The Raman spectra were carried out in a Renishaw InVia confocal microscope using an excitation wavelength of 514 nm, taking a spectrum in several areas of the sample for assuring reproducibility. The high resolution SEM images were obtained in Hitachi S-4800 N field emission gun scanning electron microscope (FEG-SEM) with an accelerating voltage of 5 kV. For the TEM analysis, the samples were crushed and dispersed in ethanol at a concentration of 4 mg ml^{-1}. A sample of the dispersion (3 μl) is placed on a grid covered with a carbon film and, after allowing to dry, the TEM images were obtained in a Jeol 1400 Plus transmission electron microscope using an accelerating voltage of 100 kV.

The dolomite used as pre-reforming catalyst for bio-oil conditioning was obtained by calcination of natural dolomite ($CaMg(CO_3)_2$, provided by *Calcinor S.A.* (Cantabria, Spain)) at 850 °C for 5 h to decompose it into the active species (CaO and MgO). The calcined dolomite was composed of 67 wt% CaO and 33 wt% MgO [61].

2.2. Bio-oils

The raw bio-oil (RB) (1.2 g ml^{-1} density) was obtained by flash pyrolysis of pine sawdust in a conical rotary reactor (BTG Bioliquids BV, The Netherlands).

The bio-oil treated by phenols removal (TB) was obtained by subjecting the RB to L-L solvent-anti-solvent extraction, using dichloromethane (DCM) as hydrophobic-polar solvent and water as anti-solvent to induce the phase separation, with a volumetric bio-oil/DCM/water ratio of 0.5/1/2, which is suitable to minimize the content of phenols in the TB (the aqueous phase resulting from the extraction). Moreover, the TB has a S/C ratio near 6, which is suitable for its reforming [52].

The raw bio-oil (RB) and the bio-oils obtained after each conditioning method (by phenols extraction (TB) and by pre-reforming with dolomite (PRB) were characterized by Karl Fischer titration (KF Titrino Plus 870) for quantifying the water content, elemental analysis (LECO CHN-932 analyzer) for determining the C, H, N, O composition, and gas chromatography/mass spectrometry (GC/MS) (QP2010S Shimadzu) for determining the detailed oxygenates composition. The GC/MS spectrometer is provided with a BPX-5 column (50 m × 0.22 mm × 0.25 μm) and mass selective detector. Identification of compounds was accomplished by matching the mass spectra with NIST 147 and NIST 27 data libraries.

2.3. Reaction equipment and operating conditions

The SR experiments were carried out in a continuous two-units automated reaction equipment (MicroActivity Reference from PID Eng&Tech) previously described [57]. The Unit 1 is a U-shaped steel tube (inner diameter = 19 mm) at 500 °C, for the vaporization of bio-oil and the controlled deposition of the pyrolytic lignin (PL) formed by repolymerization of oxygenates (mainly phenolic compounds derived from the pyrolysis of the biomass lignin). The effluent of Unit 1 enters Unit 2, consisting of a fluidized bed reactor for the oxygenates SR (22 mm of internal diameter, total length of 460 mm and effective reaction length of 10 mm). The bed consists of the catalyst (particle size of 150–250 μm to avoid internal diffusional limitations) and an inert solid (SiC, 37 μm particle size), with inert/catalyst mass ratio > 8/1 in order to ensure good fluid dynamic behaviour of the catalytic bed. Unit 1 is also used as the pre-reforming reactor for bio-oil conditioning when necessary. For this, the calcined dolomite (4 g) was placed in the outlet side (over quartz wool), for the pre-reforming at 500 °C of the bio-oil vaporized at the same temperature in the inlet side of this unit.

The bio-oil (RB or TB) was pumped at 0.08 mL min^{-1} with a Harvard Apparatus 22 injection pump, and water was co-fed pumped with a 307 Gilson pump in order to set the desired S/C ratio of 3. No additional water is pumped to the reactor in the SR of the TB. Inert N_2 was co-fed with balanced flowrate according to the required amount of water, so that total feed flowrate remains in the 800–1000 mL min^{-1} range in reforming reaction conditions (required for a suitable fluidization). The SR reactions were carried out under atmospheric pressure at 600 and 700 °C, with space–time of 0.14 $g_{catalyst}h/g_{bio\text{-}oil}$ (defined as the ratio between the catalyst weight and the flowrate of oxygenates in bio-oil fed to Unit 1). The selection of these reforming temperatures is based on a previous study [19], in which it was established that the catalyst is more stable at 600 and 700 °C than at an intermediate temperature of 650 °C. Accordingly, the coke formation is highly favored with the increase in the reforming temperature from 600 to 650 °C, causing a rapid catalyst deactivation at 650 °C. However, at 700 °C, the coke formation is

attenuated because the gasification reaction is favored with this increase in the reforming temperature. Prior to each SR experiment, the $NiAl_2O_4$ spinel was reduced *in situ* under a H_2 (10 mol%)/N_2 flow at 850 °C for 4 h, thus producing well-dispersed Ni^0 particles supported on Al_2O_3.

The composition of the reaction products exiting the fluidized bed reactor was analyzed online using a micro gas chromatograph (MicroGC 490 Agilent) provided with four columns: molecular sieve MS5 (for H_2, O_2, N_2, CH_4 and CO analysis), Plot Q (for CO_2, H_2O and C_2-C_4 hydrocarbons), CPSIL (for C_5-C_{11} hydrocarbons), and Stabilwax (for oxygenates).

The kinetic behavior was quantified according to the oxygenates conversion, and the yields of H_2 and carbon products, defined by Eqs. (11)-(13)), respectively.

$$X = \frac{F_{ox,in} - F_{ox,out}}{F_{ox,in}} \quad (11)$$

$$Y_{H2} = \frac{F_{H2,out}}{\nu_{H2} F_{Ox,in.}} 100 \quad (12)$$

$$Y_i = \frac{F_{i,out}}{F_{ox,in}} 100 \quad (13)$$

where $F_{ox,in}$ and $F_{ox,out}$ are the carbon-based molar flow-rates of oxygenates at the inlet and outlet, respectively, of the fluidized bed reactor (or the two-catalytic-step reaction system when dolomite is use as pre-reforming catalyst). $F_{ox,in}$ was calculated by subtracting the amount of PL deposited in Unit 1 from the bio-oil fed (mass balance). $F_{H2,out}$ is the H_2 flowrate in the effluent of the Unit 2 unit; ν_{H2} is the stoichiometric hydrogen mole, that is, the maximum moles of H_2 formed per mole of C in the oxygenated feed, calculated according to the overall SR reaction of oxygenates (Eq. (1)), and; $F_{i,out}$ is the carbon-based molar flowrate of the *i* product in the effluent of Unit 2.

3. Results

3.1. Effect of raw bio-oil conditioning on the oxygenates concentration

Table 1 summarizes the composition of raw bio-oil (RB) and treated bio-oil by L-L extraction (TB) before and after the separation of pyrolytic lignin (PL) at 500 °C in Unit 1 (the yields of PL obtained with each bio-oil are shown in Table 2). The comparison of the composition of both bio-oils at the inlet of Unit 1 evidences that TB has low contents of ketones, esters, aldehydes and phenols, whereas the content of furans, alcohols and saccharides increases compared to RB, mainly the latter. The phenol content decreased by 77%, confirming the efficiency of this procedure to extract phenols from raw bio-oil [52,62]. The separation of PL of RB leads to an increase in the concentration of saccharides, ketones and acids, whereas that of phenols decreases noticeably. Conversely, for the TB, the separation of PL involves a noticeable decrease in the amount of saccharides and increase in esthers, whereas phenols and acids slightly decrease and ketones increases. When comparing the composition of the oxygenates stream after the separation of PL (that is, the composition entering the reforming reactor), the main difference is a noticeable lower amount of phenols and higher amount of saccharides for the TB (3.7 and 28.9 %, respectively) than for RB (10.6 % phenols and 19.0 % saccharides).

Likewise, Table 3 summarizes the evolution with time on stream (TOS) of the composition of the stream exiting Unit 1 when it is used for the pre-reforming step, with 4 g of dolomite (space time of 0.9 $g_{dolomite}{\cdot}h{\cdot}(g_{oxygenates})^{-1}$ at 500 °C. The composition significantly changes due to the progressive deactivation of dolomite, being rich in ketones at zero time on stream but rich in phenols after 1 h, when the dolomite is saturated with CO_2. Compared to the RB feed composition (Table 1), the pre-reforming with dolomite mainly converts carboxylic acids and saccharides into ketones at the beginning of the reaction. The presence of basic sites in dolomite catalyzes ketonization, water–gas shift, steam reforming and cracking reactions depending on the reaction conditions [52]. Thus, with fresh dolomite carboxylic acids and levoglucosan conversion via ketonization reactions are the prevailing reactions, whereas when dolomite deactivates (by carbonatation and coke

Table 1
Semi-quantitative composition (% chromatographic area) of RB and TB, at the inlet and outlet of Unit 1 (separation of PL at 500 °C).

	Raw Bio-oil		Treated Bio-oil	
	inlet	outlet	inlet	outlet
Acids	**19.5**	**28.8**	**19.6**	**17.2**
Acetic	*16.6*	*20.8*	*13.4*	*15.9*
Ketones	**21.4**	**26.4**	**10.8**	**11.8**
Linear	*17.1*	*20.7*	*8.5*	*10.4*
Acetone	*5.2*	*1.0*	*0.3*	*1.2*
Acetol	*9.4*	*15.4*	–	*7.3*
Cyclic	*4.3*	*5.7*	*2.4*	*1.4*
Esters	**11.3**	**1.1**	**3.2**	**17.5**
Furans/Furanones	**5.0**	**4.4**	**9.1**	**5.5**
Alcoholes	**3.2**	**2.0**	**8.2**	**8.9**
Aldehyds	**6.8**	**6.4**	**1.0**	**4.5**
Ethers	**0.8**	**1.2**	**1.0**	**1.9**
Saccharides	**13.7**	**19.0**	**41.3**	**28.9**
Levoglucosan	*11.1*	*13.8*	*35.4*	*26.4*
Phenols	**18.4**	**10.6**	**4.3**	**3.7**
Alkyl-phenols	*1.4*	*0.7*	*0.0*	*0.4*
Guaiacols	*11.1*	*2.6*	*1.1*	*0.1*
Catechols	*0.9*	*3.5*	*2.4*	*2.9*
Other	*5.0*	*3.8*	*0.8*	*0.4*

Table 2
Yield and composition of pyrolytic lignin (PL) deposited in the thermal treatment of raw and treated bio-oil (by phenol extraction), elemental composition of the remaining bio-oils and after pre-reforming with dolomite, and value of the maximum (stoichiometric) H_2 moles (ν_{H2}) in the SR of each bio-oil.

	RB	TB	PRB
Composition	$C_{3.9}H_{6.9}O_{2.9}$	$C_{3.8}H_{5.5}O_{3.0}$	$C_{3.9}H_{6.9}O_{2.9}$
Yield of PL (wt%)	17.7	6.2	9.5
Composition of PL	$C_{6.1}H_{3.6}O_{1.5}$	$C_{7.0}H_{3.8}O_{0.7}$	$C_{6.1}H_{3.6}O_{1.5}$
Composition after deposition of PL	$C_{3.5}H_{7.6}O_{3.2}$	$C_{2.9}H_{6.3}O_{3.7}$	$C_{3.7}H_{7.2}O_{3.0}$
ν_{H2} (mol H_2/mol C)	2.18	1.8	2.16

Table 3
Evolution with time on stream of the semi-quantitative composition (% chromatographic area) of the oxygenates after the pre-reforming step (PRB). Conditions: 500 °C, 4 g dolomite, space time of 0.9 $g_{dolomite}{\cdot}h{\cdot}(g_{oxygenates})^{-1}$.

	0.5 h	1 h	2 h	3 h	4 h
Acids	**0.7**	**4.2**	**4.6**	**10.1**	**6.6**
Acetic	–	*1.8*	*3.2*	*3.4*	*2.9*
Ketones	**82.7**	**58.5**	**51.1**	**35.5**	**26.2**
Linear	*38.6*	*27.3*	*25.1*	*16.6*	*9.9*
Acetone	*22.8*	*25.7*	*18.6*	*11.3*	*7.5*
Acetol	–	*0.3*	*0.9*	*1.3*	*1.0*
Cyclic	*44.1*	*31.2*	*26.0*	*18.9*	*16.4*
Esters	**0.1**	**–**	**0.2**	**0.2**	**0.9**
Furans/Furanones	**0.4**	**1.7**	**1.9**	**3.8**	**3.9**
Alcohols	**3.3**	**2.7**	**4.7**	**4.8**	**3.7**
Aldehydes	**3.2**	**2.5**	**5.2**	**5.0**	**1.8**
Esthers	**–**	**–**	**–**	**0.1**	**0.2**
Saccharides	**–**	**4.9**	**6.1**	**10.9**	**15.7**
Levoglucosan	–	*1.9*	*2.3*	*6.3*	*10.2*
Phenols	**9.7**	**23.4**	**25.6**	**29.2**	**39.8**
Alkyl-phenols	*9.3*	*23.4*	*5.9*	*5.9*	*9.1*
Guaiacols	*0.1*	–	*1.6*	*2.2*	*8.1*
Catechols	*0.3*	–	*17.4*	*19.7*	*19.9*
Syringols	–	–	–	–	–
Naphtalenols	–	–	–	–	*0.3*
Other	–	–	*0.7*	*1.4*	*2.4*
Hydrocarbons	–	**2.1**	**0.6**	**0.4**	**1.1**
Linear	–	*2.1*	*0.6*	*0.4*	*1.1*
Cyclic	–	–	–	–	–

deposition), cracking reactions involving poly-substituted phenols are favored, leading to the formation of alkylphenols.

The calculation of the stoichiometric H_2 moles, ν_{H2}, in Eq. (12) requires determining the elemental composition (C, H and O) of the oxygenates entering the reforming step (Unit 2). This composition has been calculated by means of a mass balance, considering the elemental composition of the RB fed to the system, and the quantity and composition of LP deposited in Unit 1. The elemental composition of oxygenates before and after the separation of PL, along with the PL yield and composition are shown in Table 2 for the three bio-oils studied. The corresponding stoichiometric H_2 moles (maximum achievable per mole of C fed to the bio-oil) is included in the table. As can be seen, feeding RB leads to a much higher PL yield than feeding the TB, mainly due to the lower water content and higher content of phenolic compounds in the RB. The oxygenates stream resulting from the deposition of PL is less carbonaceous and hydrogenated for the TB, so the stoichiometric H_2 moles is significantly lower than for the SR of the RB after the separation of the PL. Applying a dolomite pre-reforming stage leads to a considerable decrease in the PL yield deposited in this unit, although its effect on the composition of the PL and the resulting PRB, as well as on the stoichiometric H_2 moles, is not significant.

3.2. Steam reforming of the bio-oils with different composition

3.2.1. Raw bio-oil (RB)

Fig. 1 shows the TOS evolution of the oxygenates conversion (graph a), yields of H_2 (graph b) and CO_2 (graph c) in the SR of RB at 600 and 700 °C, up to almost complete catalyst deactivation. The catalyst lifetime is noticeably longer at 600 °C (13 h) than at 700 °C (7.5 h).

At both temperatures, total oxygenates conversion is attained at zero TOS, with initial H_2 yield near 90%, slightly higher at 700 °C. The yield of H_2 and CO_2 decrease at both temperatures with TOS almost in parallel to the decrease in oxygenates conversion, whereas those of the rest of carbon products (Fig. S2) increase, more rapidly at 700 °C, as the SR reactions (of oxygenates, CH_4 and hydrocarbons) and WGS reaction are being affected by the deactivation of the catalyst.

3.2.2. Treated bio-oil (TB)

Fig. 2 shows the TOS evolution of the oxygenates conversion and yields of H_2 and CO_2 obtained in the SR of TB at 600 and 700 °C. The results for carbon byproducts (CO, CH_4 and hydrocarbons) are shown in Fig. S3. As observed in Fig. 2a, total conversion is attained at 700 °C, but not at 600 °C for the low value of space time used in this study, which evidences the lower reactivity of the TB compared to RB. Accordingly, the H_2 yield is noticeably lower at 600 °C (72 %) than at 700 °C (92 %).

In comparison with the SR of RB, the stability of the catalyst in the SR of TB (Fig. 2) is noticeably higher at 700 °C than at 600 °C. Thus, at 700 °C the oxygenates conversion and product yields remain fairly stable for almost 3 h on stream, and thereafter a moderate decrease in conversion and H_2 and CO_2 yields is observed. Conversely, at 600 °C there is a rapid decrease in the conversion and H_2 and CO_2 yields, so that the catalyst is almost completely deactivated after 150 min on stream. The nearly constant yield of CO at 600 °C (Fig. S3a) is explained by a similar rate of deactivation of the SR (CO forming, Eq. (2)) and WGS (CO converting, Eq. (3)) reactions [42]. It should be noted that, in order to correctly interpret the rapid deactivation observed at 600 °C in Fig. 2, the incomplete conversion of oxygenates should be taken into account, as this situation leads to a very rapid coke deposition (Eq. (4)) [19].

3.2.3. Pre-reformed bio-oil (PRB)

Fig. 3 compares the oxygenates conversion and yields of H_2 and CO_2 in the SR of PRB at 600 and 700 °C. For a better interpretation of the results, the conversion and product yields at the outlet of the pre-reforming step (corresponding to the activity of dolomite) are also included in the graphs (continuous lines). At both reforming temperatures total oxygenates conversion is attained at zero TOS (Fig. 3a), but

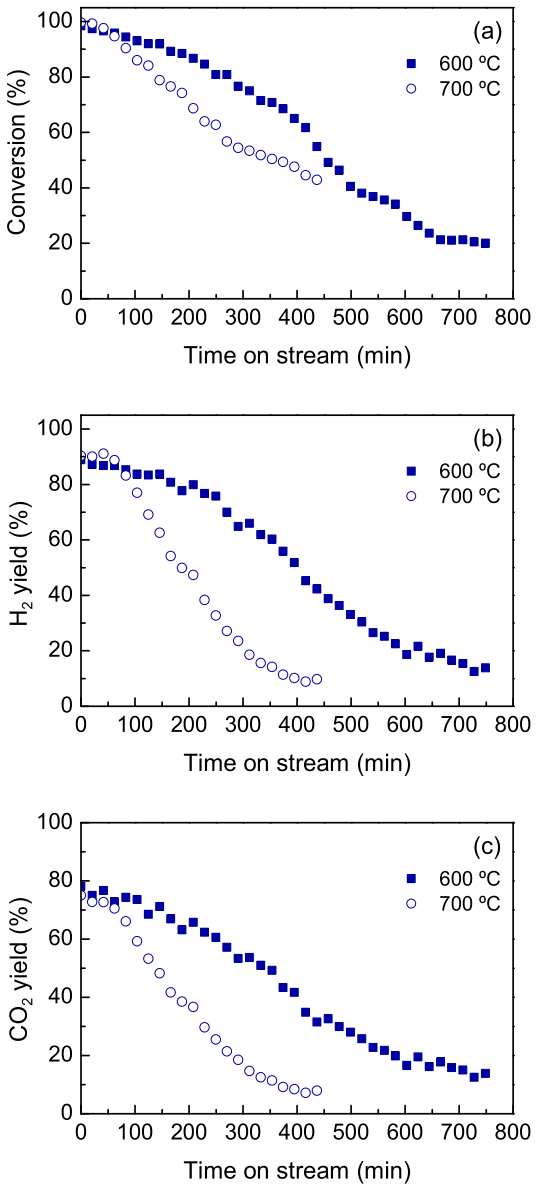

Fig. 1. Time on stream evolution of the (a) oxygenates conversion and yields of (b) H_2 and (c) CO_2 for the SR of raw bio-oil (RB) at 600 °C and 700 °C.

with different H_2 yield (Fig. 3b), being higher at 700 °C (~80 %) than at 600 °C (~70 %). This difference evidences that the increase in temperature favors SR reactions over the cracking/decomposition reactions of oxygenates. The higher extent of SR reactions at 700 °C is also evidenced by the higher initial CO yield at 700 °C than at 600 °C (Fig. S4a), despite the fact that the reverse WGS reaction is thermodynamically favored at elevated temperature.

The temperature also affects the catalyst stability. At 700 °C, conversion remains almost constant for about 1 h, probably due to the excess of catalyst with respect to the minimum necessary to achieve total conversion. Afterwards, there is a rapid and progressive decrease in the conversion and yield of H_2, whereas those of CH_4 and hydrocarbons increase (Figs. S3b and S4c), reaching almost total deactivation after 4 h on stream. The peculiar evolution of the yields of CO_2 and CO (Fig. 3c and S4a, respectively), with a rather stable period in the first 50 min, followed by a rapid increase between 50 and 75 min, is a consequence of the saturation of dolomite with CO_2 in the pre-reforming step at that time on stream, as evidenced by the continuous line in Fig. 3c [53]. The oxygenates conversion at 6 h TOS (near 55 %) is higher than that

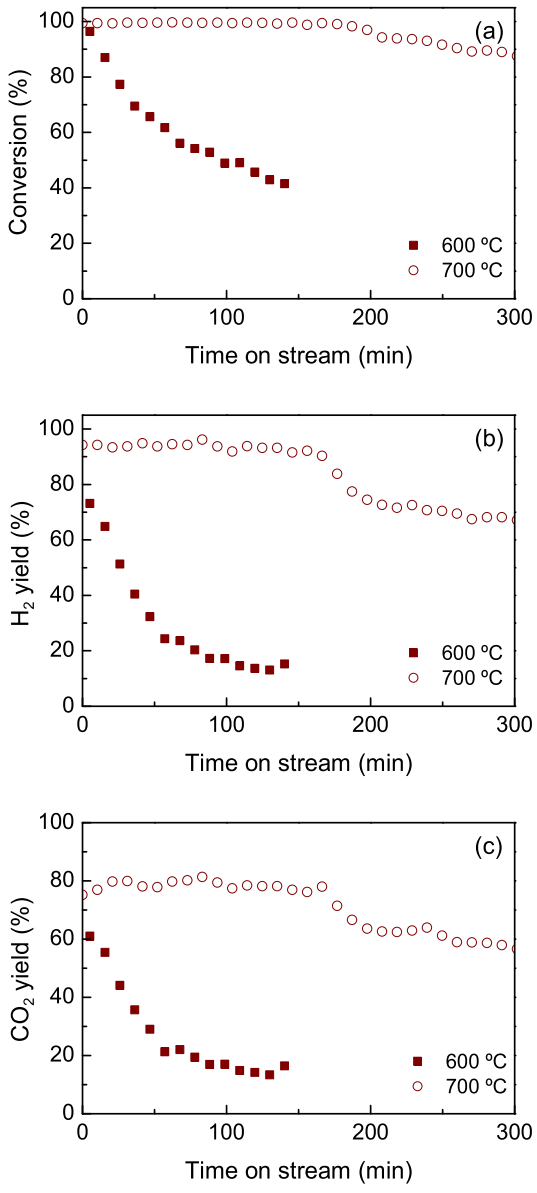

Fig. 2. Time on stream evolution of the (a) oxygenates conversion and yields of (b) H_2 and (c) CO_2 for the SR of treated bio-oil (TB) at 600 °C and 700 °C.

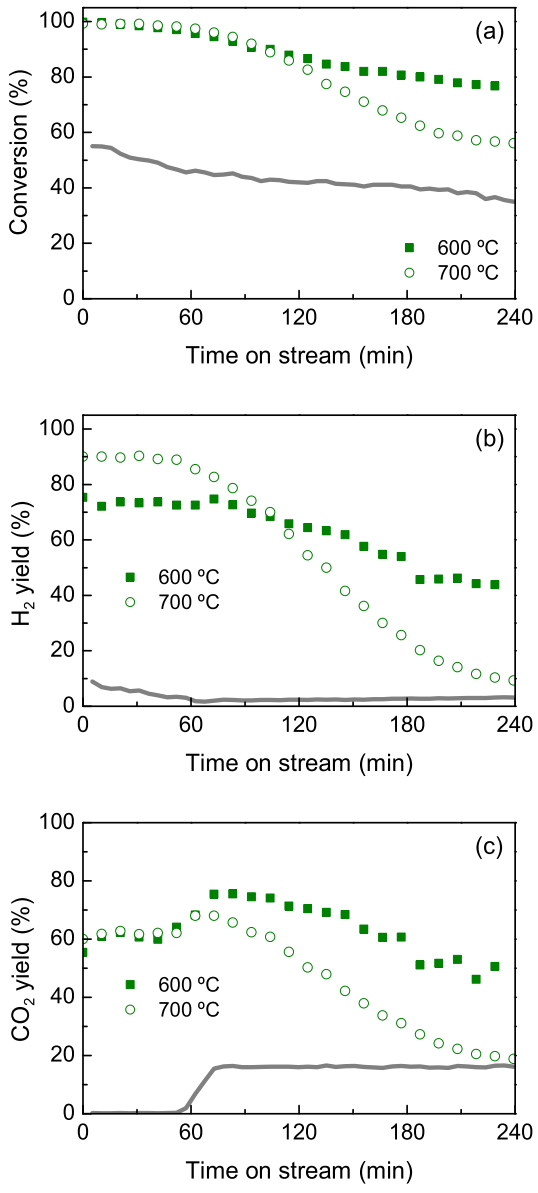

Fig. 3. Time on stream evolution of the (a) oxygenates conversion and yields of (b) H_2 and (c) CO_2 for the pre-reformed bio-oil (PRB) with dolomite and subsequent SR on the $NiAl_2O_4$ derived catalyst at 600 °C and 700 °C. Lines: reaction indices at the outlet of pre-reforming step.

obtained in the pre-reforming step with dolomite (near 35 %) due to the higher temperature in the reforming reactor, and the low yields of H_2 and CO_2 are similar to those obtained by thermal cracking of raw bio-oil at this temperature [31], thus evidencing that the catalyst is almost completely deactivated. Conversely, at 600 °C the oxygenates conversion decreases with TOS, but more slowly than at 700 °C, so that after 4 h the catalyst remains partially active with a significant oxygenates conversion and H_2 yield (75 % and 42 %, respectively). Consequently, the SR of the PRB at 600 °C leads to a more stable H_2 production than at 700 °C, similarly to that observed in the SR of RB.

When comparing the afore mentioned results for the three bio-oil feeds at a given temperature, the catalyst stability in the SR at 600 °C follows the order RB > PRB ≫ TB, whereas at 700 °C the order of stability is TB ≫ RB > PRB. The relevant difference among all the experiments at a given temperature is the bio-oil composition. Phenols are well known coke precursors and accelerate coke formation leading to catalyst deactivation [56] and, therefore, it is expected that the removal of phenols attenuates coke formation [52]. Nevertheless, our results suggest that this effect is opposite at a reforming temperature of 600 °C, which may be attributable to a particular effect of temperature on coke characteristics. Thus, in the next sections, we further investigate the used catalyst samples in order to analyze the coke characteristics and their impact on catalyst deactivation.

3.3. Analysis of spent catalyst

3.3.1. XRD analysis

Fig. 4 shows the XRD patterns of the fresh catalyst and the catalysts used in the SR of the different bio-oils at 600 °C (graph a) and 700 °C (graph b), providing their structural characteristics. In general, all the patterns show similar peaks assigned to Al_2O_3 phases (2θ = 37.5, 46.0 and 67.1°) and Ni^0 crystals (2θ = 46.7 and 52.0°), which evidences the absence of Ni oxidation in the used catalyst samples.

The peak at 2θ = 52.0° was used to determine the average Ni^0 crystallite size through the Scherrer equation, and Table 4 lists the results. The average Ni^0 crystallite size does not significantly change from the fresh catalyst to the used catalysts, indicating that sintering

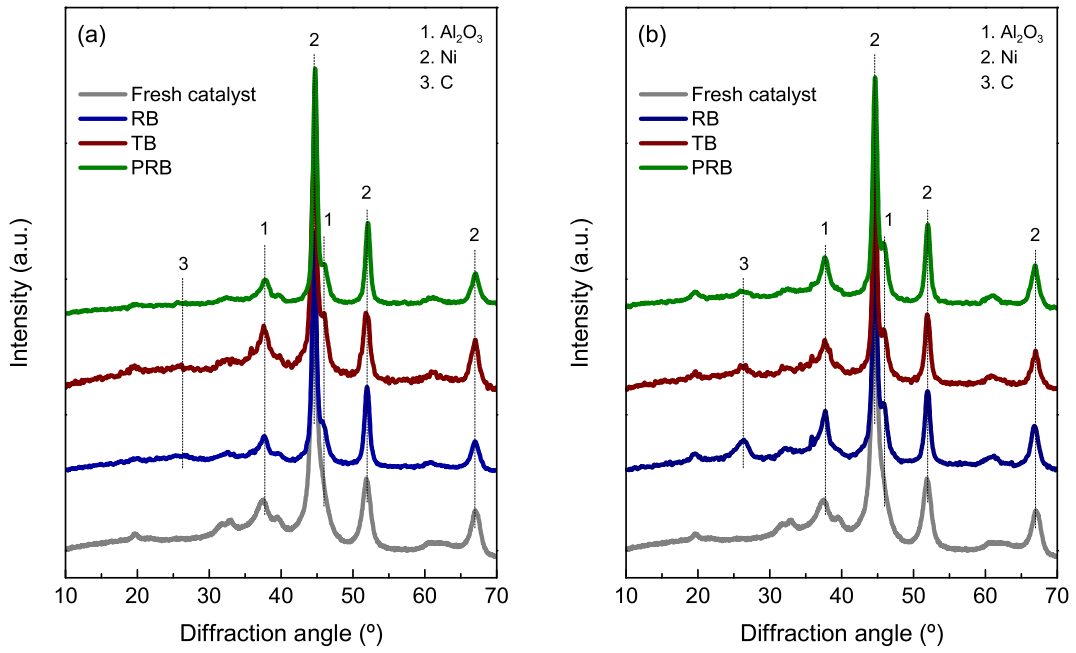

Fig. 4. XRD patterns of the fresh catalyst and catalysts used in the SR of raw bio-oil (RB), treated bio-oil (TB) and pre-reformed bio-oil (PRB) at 600 °C and 700 °C.

Table 4
Average Ni^0 crystallite size, total coke content and of each coke fraction and average deposition rate (r_c) for the catalyst used in the SR at 600 °C and 700 °C of the different bio-oils.

		Ni^0, nm	C_c, wt% Total	Coke I	Coke II	r_c, wt% h^{-1}
	Fresh	13	–	–	–	–
Raw Bio-oil	700 °C	11	15.7	0.55	15.17	2.1
	600 °C	12	17.6	13.70	3.92	1.4
Treated bio-oil	700 °C	12	8.8	0.32	8.52	1.8
	600 °C	11	7.2	1.40	5.78	2.9
Pre-reformed bio-oil	700 °C	12	9.4	0.57	8.86	2.2
	600 °C	13	9.7	7.86	1.81	2.3

phenomenon did not take place to a significant extent. Additionally, the XRD patterns of the catalysts used at 700 °C (more noticeably those with RB or TB) show a peak at $2\theta = 26°$ indicative of crystalline carbon structures [56,63]. Nevertheless, this peak intensity is low indicating the poor degree or content of crystalline carbon structures.

3.3.2. Coke TPO

Fig. 5 shows the TPO profiles of the catalysts used in the SR of the different bio-oils at 600 °C (graph a) and 700 °C (graph b). The coke combustion takes place at two different temperature ranges: coke burning below 500 °C that is named coke I, and coke burning above 500 °C named coke II. Coke I is the prevailing fraction in the TPO profiles of catalysts used in the SR at 600 °C of RB and PRB, whereas coke II is the major fraction for the rest of the used catalyst samples. Based on the composition of the bio-oils, the low content of coke I in the catalyst used in the SR of TB at 600 °C corroborates the relevant role of phenols in its formation [56].

Additionally, Table 4 summarizes the total coke content and partial content of coke I and II calculated by numerically integrating the TPO profiles (area under the curve). The average coke deposition rate is calculated assuming a constant deposition rate. The results evidence a significant lower total coke content in the SR of TB and PRB compared with RB, although this result could be attributed mainly to the longer duration of the experiments in the SR of the RB, since the coke deposition rate values show a high uniformity, with no clear trend depending

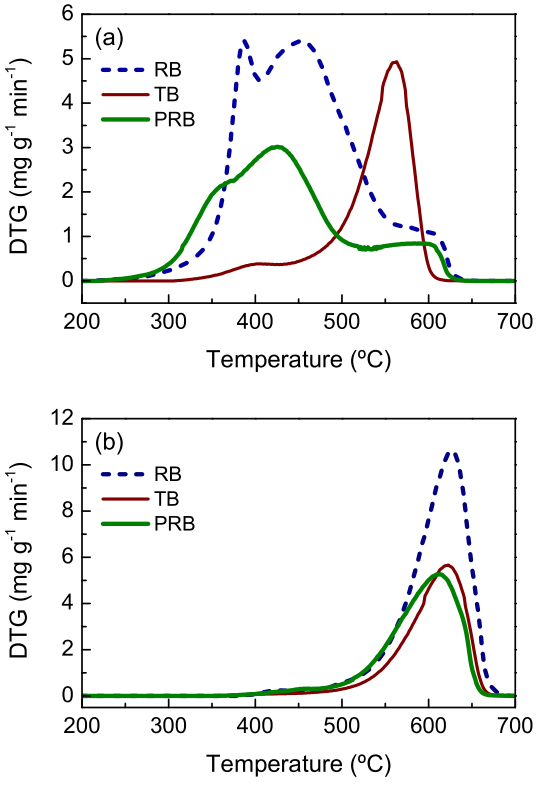

Fig. 5. TPO profiles of the catalysts in the SR of raw bio-oil (RB), treated bio-oil (TB) and pre-reformed bio-oil (PRB) at (a) 600 °C and (b) 700 °C.

on the composition of the feed to be reformed. The reforming temperature does not significantly affect the total coke content, but it has a relevant impact on its nature and, to a lower extent, on the average coke deposition rate, this effect being different depending on the composition of bio-oil. Thus, in the SR of the TB, with mostly coke II at both 600 and 700 °C, increasing the reforming temperature leads to a significant decrease in the average coke deposition rate, which is consistent with

increased coke gasification (Eq. (10)) at elevated temperature. However, the average coke deposition rate apparently increases with temperature in the SR of RB, and hardly varies in the SR of PRB. These different results may be attributed to the different nature of the coke deposited in the SR of RB and PRB (mostly coke I at 600 °C and coke II at 700 °C), compared to the SR of TB (mostly coke II at any temperature) and to a different gasification capacity of their coke fractions. These differences are consequence of the different oxygenates composition in the bio-oils.

Based on the these results, the values of total coke content and average coke deposition rate in Table 4 do not correlate directly with the deactivation rate observed in Figs. 1-3, which evidences a different deactivation capacity of the different coke fractions. Thus, the fastest deactivation rate observed for the SR at 600 °C of the TB (Fig. 2) is consistent with the fastest coke deposition rate in Table 4 (mostly coke II). However, in the SR of the PRB the deactivation rate is lower at 600 °C than at 700 °C, despite the slightly higher average coke deposition rate. This result highlights the lower deactivating capacity of coke I formed in the SR of the PRB compared to coke II, as previously reported for the SR of RB [19]. According to this previous work, the deposition of coke II leads to faster deactivation of the catalyst by blocking both the Ni sites in the surface (active for the reforming) and the Al_2O_3 support sites (active for water adsorption and dissociation), an important step in the SR. This effect is presumably more important at lower temperature, when there is incomplete oxygenate conversion, which leads to the high deactivation rate observed in the SR at 600 °C of the TB (Fig. 2), with mostly coke II (Table 4).

3.3.3. Raman spectroscopy

Fig. 6 shows the Raman spectra of the catalyst used in the SR of the bio-oils at 600 °C (graph a) and 700 °C (graph b), providing further information on the coke structure characteristics. At first glance, the spectra show common features with two relevant bands at ~ 1340 cm^{-1} (D band) and ~ 1580 cm^{-1} (G band) that are typical of several carbon structures [64]. To obtain more information from the Raman spectra, Fig. 6c shows an example of the deconvolution of the Raman spectrum into four Lorentzian bands applied to the spectra of all the used catalyst samples. The assignation of these bands is as follows [19,56,65,66]: ~1200 cm^{-1} (D4), vibration mode of sp^3-hybridized carbon; ~1340 (D) sp^2-hybridized carbon in aromatics; ~1500 cm^{-1} (D3), phases of amorphous carbon; ~1580 cm^{-1} (G), sp^2-hybridized carbon in aromatics and chains.

Among all the typical parameters provided from the deconvolution results, we found that the D/G intensity ratio and the full-width at half-maximum (FWHM) of the D3 band (amorphous carbon phases) can be correlated with the mean coke combustion temperature (MCCT) obtained as the weighted average of the TPO profile and which indicates the feasibility of coke removal by combustion. The D/G ratio intensity increases with the increase in the MCCT (Fig. 6d, right vertical axis). The development of the D band indicates order in amorphous carbons [65], and in this case the D/G ratio is proportional to the cluster size (L_a) of ordered carbon domains. Thus, the increase in the D/G ratio indicates the formation of more ordered carbon structures, which is coherent with the increase in the MCCT. Likewise, the FWHM of the D3 band decreases with the increase in the MCCT (Fig. 6d, left vertical axis). Hence, the lower presence of amorphous carbon in coke directly increases the coke combustion temperature. Both correlations indicate that the formation of more ordered carbon structures (less amorphous carbon phases) increases the MCCT.

3.3.4. SEM analysis

Fig. 7 shows the SEM images with a backscattered electron (BSE) detector of the fresh catalyst (image a) and catalysts used in the SR of the bio-oils (images b-g). These images provide information on the extent of coke deposition on the external surface of the catalyst particles based on the brightness level: bright particles indicate a major presence of heavy elements such as Ni and Al, whereas dark particles indicate a major presence of light elements such as carbon [19]. Thus, the catalyst particles of the fresh catalyst (image a) are bright accounting for the

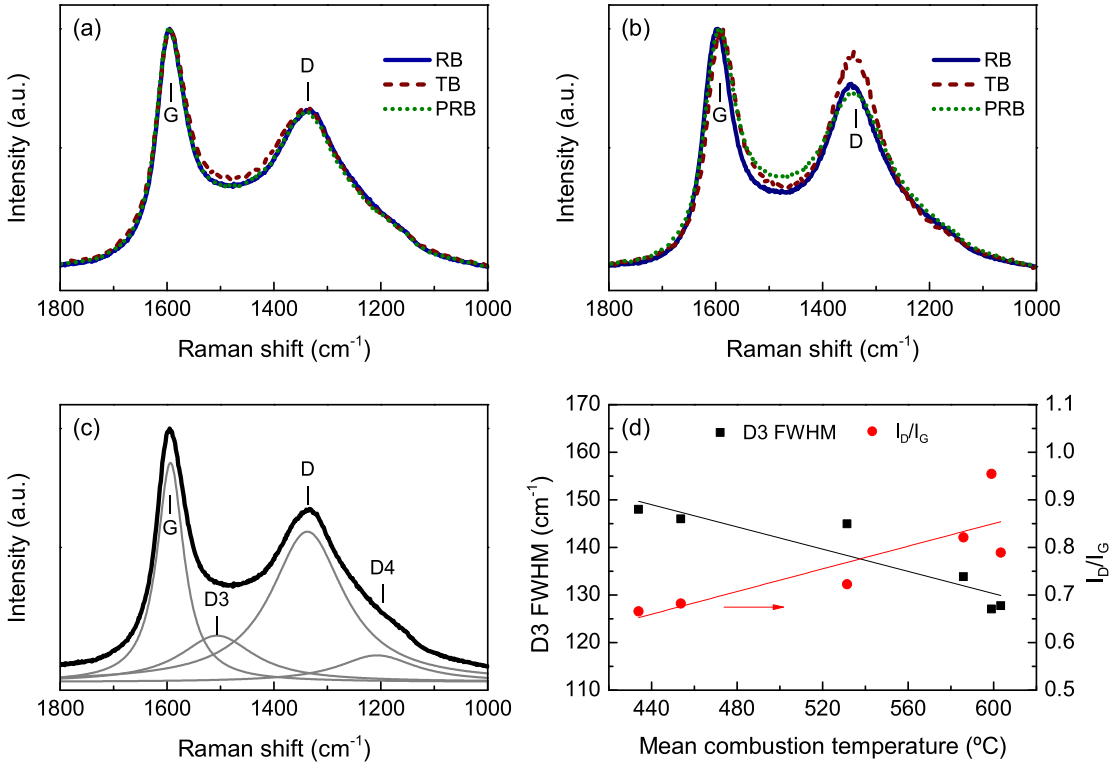

Fig. 6. Raman spectra of the catalysts used in the steam reforming of raw bio-oil (RB), treated bio-oil (TB) and pre-reformed bio-oil (PRB) at (a) 600 °C and (b) 700 °C, and (c) deconvolution of Raman spectrum and (d) correlation of Raman parameters with mean coke combustion temperature in the TPO profile.

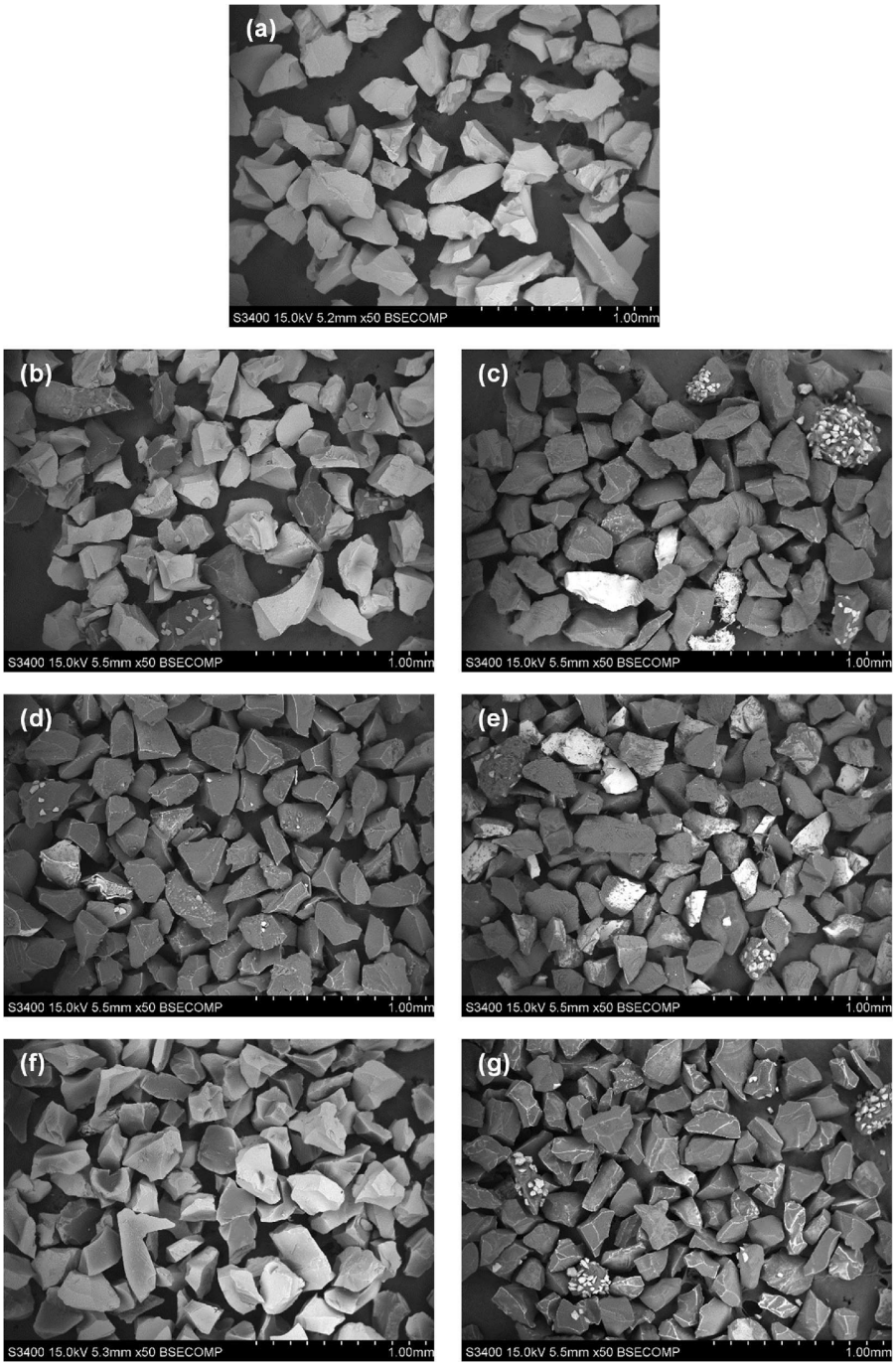

Fig. 7. BSE-SEM images of the (a) fresh catalyst and catalysts used in the SR of raw bio-oil (RB) at (b) 600 and (c) 700 °C, treated bio-oil (TB) at (d) 600 and (e) 700 °C, and pre-reformed bio-oil (PRB) at (f) 600 and (g) 700 °C.

presence of Ni and Al. The presence of semi-bright particles in the catalyst particles after the SR of RB and PRB at 600 °C (images b and f, respectively) indicates a poor coke deposition on the external surface. In contrast, the almost homogeneous dark color of the catalyst particles after the SR of TB at 600 °C (image d) and of all feeds at 700 °C (images c, e, g for RB, TB and PRB, respectively) indicates a strong coke deposition on the external surface.

Curiously, the total coke content (Table 4) is not particularly low for the samples with an apparent low carbon deposition on the external surface, and actually, the catalyst used in the SR of RB at 600 °C has the highest coke content. Additionally, these samples are the unique that show a predominant presence of coke I (Fig. 5) that presumably corresponds to less developed carbon structures (Fig. 6). These facts lead to infer that the coke formed and deposited in the SR of RB or PRB at 600 °C is mostly amorphous carbon that may be predominantly located on the internal surface of the catalyst particle (inside the pores) with some development of carbon structures on the external surface. In contrast, the coke formed and deposited in the SR of TB at 600 and 700 °C and of RB and PRB at 700 °C would be preferentially located on the external surface of the catalyst particles being composed of more developed carbon structures. The location of carbon formation may condition the carbon growth and structuration.

To study in detail the morphology of coke on the external surface, SEM images using a secondary electron detector were also taken on specific spots of a particle. Figs. 8 and 9 show the SEM images of the catalysts used in the SR of the three bio-oils at 600 °C and 700 °C,

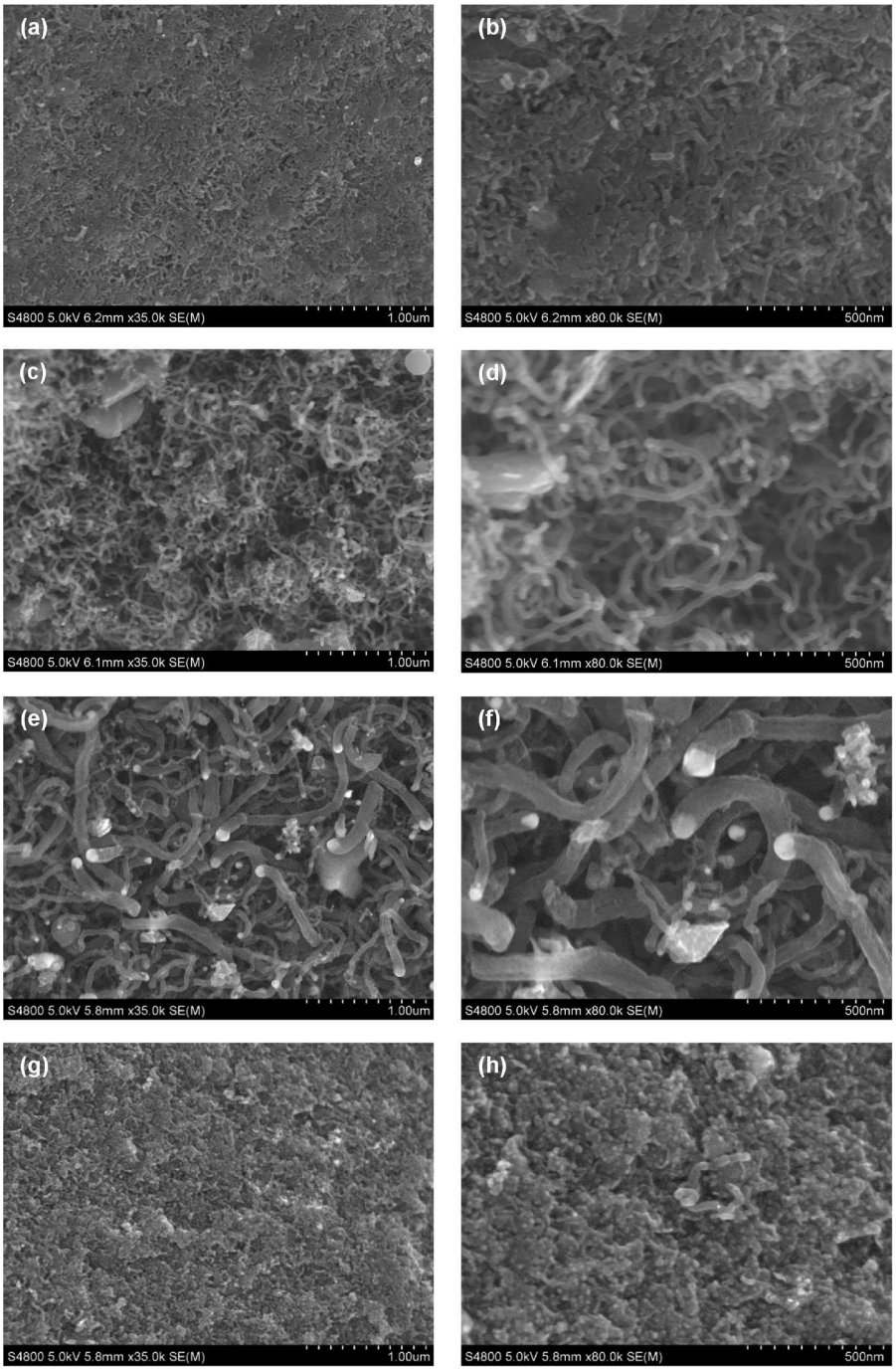

Fig. 8. SEM images at different magnifications of the catalysts used in the SR of (a-d) raw bio-oil (RB), (e-f) treated bio-oil (TB), and (g-h) pre-reformed bio-oil (PRB) at 600 °C.

respectively. Fig. S5 shows SEM images for fresh-reduced catalyst for comparison. In general, all the images reveal the great heterogeneity of the carbon morphology with a predominant formation of short and irregular carbon filaments, with different lengths and diameters, most of which are atypical from those normally observed on other catalysts for the SR of pure oxygenates [20,42,67].

At 600 °C, the catalyst after the SR of RB apparently comprises two particle types (dark and semi-bright particles in Fig. 7b) whose surface is analyzed in more detailed in Fig. 8. The external surface of the dark particles (image a-b) is covered with carbon filaments, whereas that of the semi-bright particles (image c-d) presents an amorphous and porous mass with few short carbon filaments, indicating the coke deposition is poorly dense. Thus, a high fraction of coke may be located inside the catalyst particles. In contrast, the catalyst particles after the SR of TB (images e-f) are more homogeneous and the external surface is predominantly covered with carbon filaments that are well-defined and heterogeneous in size with remarkable larger diameters than those formed in the SR of RB (image b-c).

Additionally, the images show nanoparticles (clearer zones) on the tip of the carbon filaments, corresponding to the presence of heavier elements (Al or Ni). These nanoparticles may be catalyst fragments, indicating that the formation of large carbon filaments from TB partially fragmented the catalyst particle. The growth of these large filaments can easily block the access to the internal surface of the catalyst particle and encapsulate Ni crystals. On the other hand, the surface of the catalyst used in the SR of PRB (images g-h) does not clearly show abundant

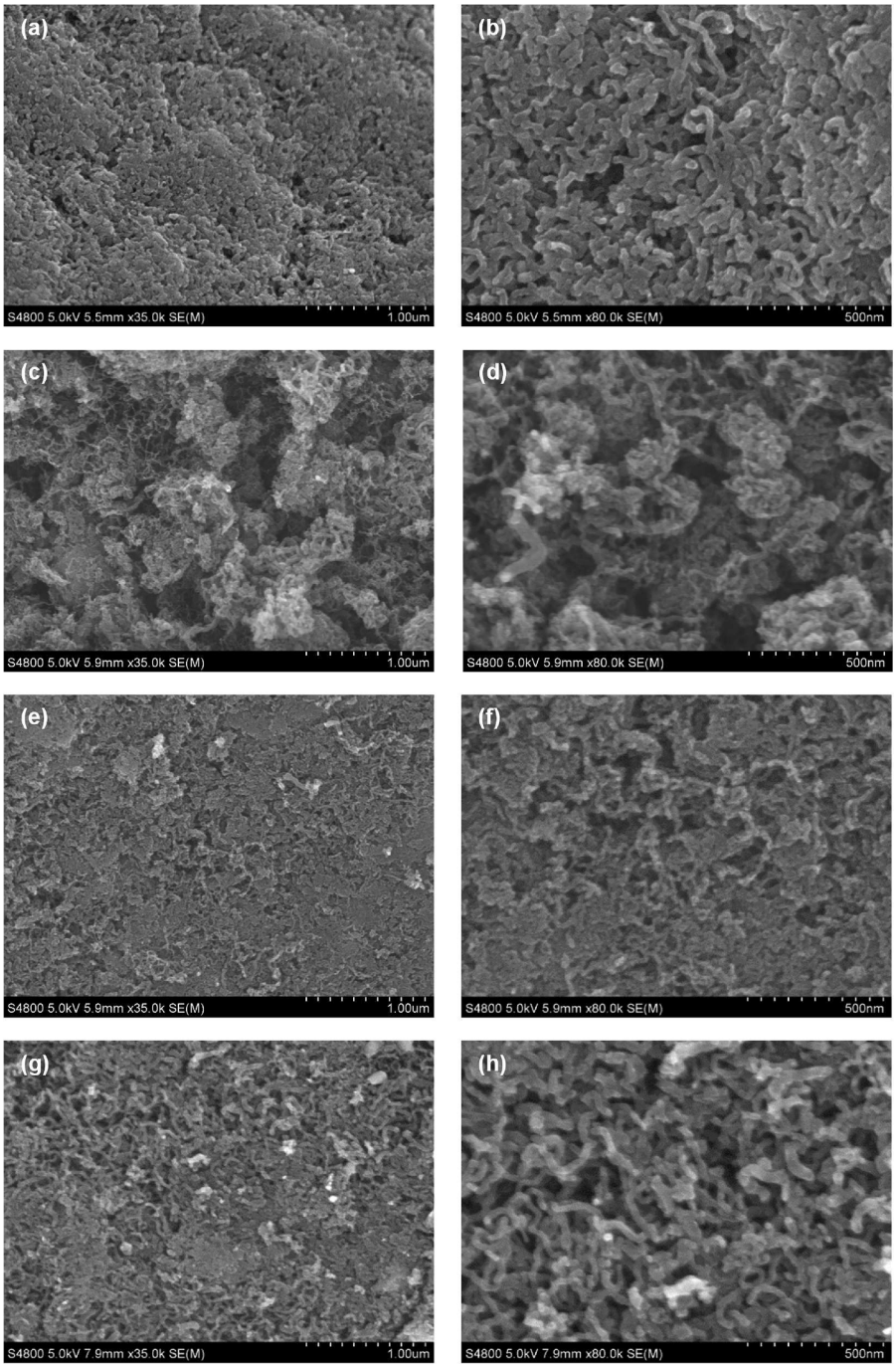

Fig. 9. SEM images at different magnifications of the catalysts used in the SR of (a-b) raw bio-oil (RB), (c-f) treated bio-oil (TB) and (g-h) pre-reformed bio-oil (PRB) at 700 °C.

carbon filaments as on the other used catalyst samples. The surface apparently resembles the morphology of the fresh catalyst (Fig. S4), and the few carbon filaments observed seem to come out from inside the particle. Thus, the coke formed from PRB at 600 °C may be composed of amorphous carbon preferentially located inside the catalyst particles.

In the SR at 700 °C (Fig. 9), the surface of the catalysts used in the SR of RB (images a-b), TB (image e-f) and PRB (image g-h) shows compacted carbon filaments. Its formation may be attributable to the deposition of another carbon phase among the filaments [19]. Interestingly, these used catalyst samples also show a peak of crystalline carbon in the XRD patterns, (Fig. 4) being more evident for the catalyst used in the SR of RB that has the highest coke content at 700 °C. Thus, the carbon phase deposited among the carbon filaments may consist of a turbostratic carbon whose formation is favored at high temperature (700 °C), containing graphite-like domains. The presence of this turbostratic carbon agglomerating the carbon filaments increases the coke combustion temperature as verified with the TPO measurements (Fig. 5). However, not all the carbon filaments from PRB (images g-h) seemingly show this compacted appearance, and therefore the complete deactivation observed may also be explained by the Ni encapsulation in the carbon filaments. In contrast, besides compacted carbon filaments, the catalyst used in the SR of TB also has particles with a different coke morphology comprised of a tangle of small carbon filaments (image c-d). Thus, these particles may remain active for SR reactions because the presence of these small carbon filaments does not block the access to the catalyst active sites [20].

TEM images were also taken on the samples of the spent and fresh catalysts (Figures S6-S8). This analysis confirm the presence and particular characteristic of carbon filaments, but no further information could be obtained since the carbon content in the catalyst particles is relatively low. In addition, the way in which these kind of samples are often treated for TEM analysis (crushing and suspension in a solvent, where only the suspended very tiny particles are the ones analyzed) makes difficult the interpretation of the observations.

4. Discussion

The results in section 3 show the important combined effect of the treatment applied to modify the bio-oil composition aiming at reducing the concentration of phenolic compounds and the reforming temperature on the Ni catalyst deactivation. In addition, the nature and location of coke also have a determining role on the deactivation rate.

After a pre-reforming step with dolomite, no significant differences were observed in the stability of the catalyst (Figs. 1 and 3) or in the coke nature (Fig. 5) or its morphology (Figs. 8 and 9) in the SR of pre-reformed bio-oil (PRB) compared to the SR of the raw bio-oil (RB). For both bio-oils, a more stable operation is obtained at 600 °C than at 700 °C. At 600 °C, coke is mostly composed of amorphous carbon preferentially formed and deposited on the internal surface of the catalyst particles. However, some carbon filaments are also abundantly formed on the external surface of few catalyst particles in the SR of RB.

At 700 °C, the coke formed in the SR of these bio-oils is composed of two coke types, made up of carbon filaments and turbostratic carbon deposited in between the filaments (Fig. 9a-b, 9 g-h). This joint deposition of two types of coke at 700 °C would cover the catalyst surface causing a rapid deactivation in comparison with that at 600 °C. The slightly faster deactivation in the SR of the PRB than that of RB, may be related to a faster coke deposition rate in the first case (Table 4), due to the progressive increase in the composition of phenolic compounds, especially after 1 h of reaction (after saturation of the dolomite with CO_2) (Table 3), which may accelerate the formation of turbostratic carbon.

In contrast, in the SR of the treated bio-oil (TB), obtained by L-L extraction of phenols from RB with DCM and water, a remarkable change is observed in the nature and morphology of the deposited coke (Fig. 8e-f and 9c-d), which results in a significant change in the stability of the catalyst in the SR reaction at different reforming temperatures (Fig. 2). These changes should be attributed to the significant decrease in the content of phenols (especially guaiacols), and increase of saccharides (mainly levoglucosan), esters and alcohols. At 600 °C, coke is predominantly composed of carbon filaments that are exceptionally large in size and may possibly lead to encapsulation of Ni crystals and access blockage to the internal surface of the catalyst particle, thus causing rapid deactivation. At 700 °C, some catalyst particles have similar coke morphology as those after the SR of RB and PRB, but most of the particles have a tangle of small carbon filaments that causes no significant deactivation, which explains the high catalyst stability observed. Consequently, the formation of deactivating carbon structures (amorphous carbon) would be greatly slowed down due to the low content of phenols, which prolongs the catalyst lifetime.

According to the observations of this work, a formation mechanism of different types of carbon structures can be stablished based on the bio-oil composition and reforming temperature (Fig. 10). Most of the oxygenates present in bio-oil (ketones, alcohols, carboxylic acids, aldehydes, saccharides) are easily reformed producing H_2, other carbon byproducts (CO, CO_2, CH_4 and olefins). These carbon byproducts are intermediates for the formation of carbon filaments (f-C) through the CO disproportionation reaction (Eq. (9)) and hydrocarbon decomposition reactions (Eqs. (7) and (8)). This carbon morphology usually has a poor effect on catalyst deactivation as demonstrated in this work and other works in the literature [20,54,67–69]. However, an uncontrolled growth of f-C (occurring at low temperature, 600 °C) may generate large filaments (mostly with large diameters) that are able to block or encapsulate the Ni sites. The increase in the reforming temperature may attenuate this f-C growth by disfavouring some formation reactions (e.g. CO disproportionation) and favouring gasification reactions (Eq. (10)) contributing to prevent the formation of large f-C. Likewise, the f-C formed at higher temperature are more refractory because dehydrogenation reactions are also favoured, making these carbon structures more dehydrogenated.

On the other hand, phenolic compounds may directly undergo condensation reactions at any reforming condition [70], which leads to the formation of polymeric structures that evolve to different carbon structures according to the reforming temperature: amorphous carbon (a-C) at 600 °C and turbostratic carbon (t-C) at 700 °C. The formation of t-C may occur due to the favoured dehydrogenation reactions at high temperatures, which yields this highly dehydrogenated carbon structure with ordered (graphitic) domains. Both a-C and t-C structures have a strong effect on catalyst deactivation because they cover the catalyst surface blocking the access to the active sites.

Therefore, the increase in the concentration of phenolic compounds favours the phenol condensation reaction and may compete with the reforming reaction of phenols. Thus, if the phenol condensation reaction is favored, the catalyst undergoes rapid deactivation by the formation of a-C or t-C. Hence, decreasing the concentration of phenolic compounds in the feed may supress the undesired condensation reaction, which requires an effective strategy to remove them.

5. Conclusions

The results of this work establish that the deactivation of the $NiAl_2O_4$ derived catalyst in the SR of bio-oil depends on the nature and location of the coke more than on the amount of coke deposited. The coke characteristics are strongly affected by both the bio-oil composition and

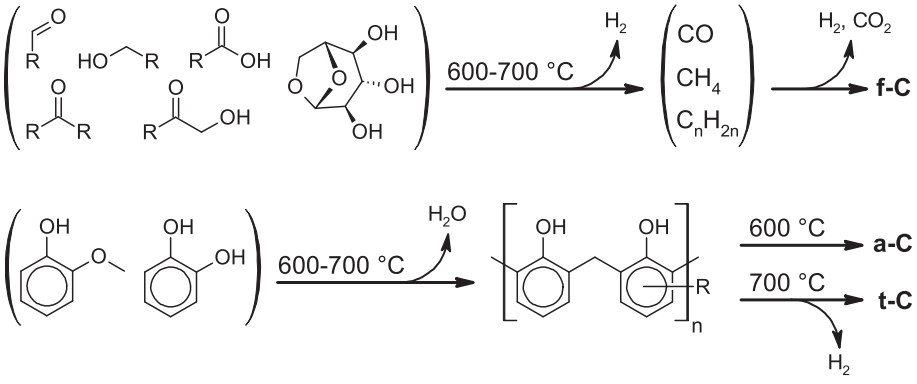

Fig. 10. Proposed mechanism for the formation of different carbon structures from different bio-oil components and reforming conditions.

reforming temperature, where phenolic compounds are mainly responsible for the carbon formation and deposition that causes the catalyst deactivation. Consequently, appropriate bio-oil modification strategies to mitigate deactivation should be aimed at reducing the concentration of phenolic compounds, but the benefit of using such strategy will depend on the reforming temperature. The best combination of strategy and reaction conditions is the L-L extraction of phenols from the bio-oil and subsequent steam reforming of the treated bio-oil at 700 °C.

With this combination, the bio-oil conversion and hydrogen yield remain stable for a long operating period. This stability is due to the coke characteristics consisting of small filaments in a tangle-like deposition that allows the diffusion of reactants to the active sites. However, the formation of deactivating turbostratic carbon is also observed in some particles, but its formation rate is slowed down due to the low content of phenolic compounds, which results in a prolonged catalyst lifetime.

Declaration of Competing Interest

The authors declare that they have no known competing financial interests or personal relationships that could have appeared to influence the work reported in this paper.

Acknowledgment

This work has been carried out with the financial support of the grant RTI2018-100771-B-I00 and PhD grant BES-2016-078132 (N. García-Gómez) funded by MCIN/AEI/10.13039/501100011033 and by "ERDF A way of making Europe", the European Commission (HORIZON H2020-MSCA RISE 2018. Contract No. 823745) and the Department of Education, Universities and Investigation of Basque Government (Projects IT1218-19 and IT1645-22). The authors thank for technical and human support provided by SGIker (UPV/EHU/ERDF, EU), and to Calcinor S.A. for supplying the dolomite.

Appendix A. Supplementary data

Supplementary data to this article can be found online at https://doi.org/10.1016/j.fuel.2022.124966.

References

[1] Sharma R, Kodamana H, Ramteke M. Multi-objective dynamic optimization of hybrid renewable energy systems. Chem Eng Process - Process Intensif 2022;170. https://doi.org/10.1016/j.cep.2021.108663.
[2] Espegren K, Damman S, Pisciella P, Graabak I, Tomasgard A. The role of hydrogen in the transition from a petroleum economy to a low-carbon society. Int J Hydrogen Energy 2021;46:23125–38. https://doi.org/10.1016/J.IJHYDENE.2021.04.143.
[3] Arregi A, Amutio M, Lopez G, Bilbao J, Olazar M. Evaluation of thermochemical routes for hydrogen production from biomass: A review. Energy Convers Manag 2018;165:696–719. https://doi.org/10.1016/j.enconman.2018.03.089.
[4] Lepage T, Kammoun M, Schmetz Q, Richel A. Biomass-to-hydrogen: A review of main routes production, processes evaluation and techno-economical assessment. Biomass Bioenergy 2021;144:105920. https://doi.org/10.1016/j.biombioe.2020.105920.
[5] Kim S-H, Kumar G, Chen W-H, Khanal SK. Renewable hydrogen production from biomass and wastes (ReBioH2-2020). Bioresour Technol 2021;331:125024. https://doi.org/10.1016/j.biortech.2021.125024.
[6] Nabgan W, Tuan Abdullah TA, Mat R, Nabgan B, Gambo Y, Ibrahim M, et al. Renewable hydrogen production from bio-oil derivative via catalytic steam reforming: An overview. Renew Sustain Energy Rev 2017;79:347–57. https://doi.org/10.1016/j.rser.2017.05.069.
[7] Shan T, Anto S, Mathimani T, Brindhadevi K, Pugazhendhi A. Upgrading of bio-oil from thermochemical conversion of various biomass – Mechanism, challenges and opportunities. Fuel 2021;287:119329. https://doi.org/10.1016/j.fuel.2020.119329.
[8] Kumar R, Strezov V. Thermochemical production of bio-oil : A review of downstream processing technologies for bio-oil upgrading, production of hydrogen and high value-added products Oil in Water. Renew Sustain Energy Rev 2021;135:110152. https://doi.org/10.1016/j.rser.2020.110152.
[9] Baloch HA, Nizamuddin S, Siddiqui MTH, Riaz S, Jatoi AS, Dumbre DK, et al. Recent advances in production and upgrading of bio-oil from biomass: A critical overview. J Environ Chem Eng 2018;6:5101–18. https://doi.org/10.1016/j.jece.2018.07.050.
[10] Xu Q, Feng P, Huang K, Xin S, Wei T, Liao L, et al. Research of the combined reforming of bio-oil model compound for hydrogen production. Environ Prog Sustain Energy 2020;39:1–9. https://doi.org/10.1002/ep.13320.
[11] Adeniyi AG, Otoikhian KS, Ighalo JO. Steam Reforming of Biomass Pyrolysis Oil: A Review. Int J Chem React Eng 2019;17. https://doi.org/10.1515/ijcre-2018-0328.
[12] Valle B, Remiro A, García-Gómez N, Gayubo AG, Bilbao J. Recent research progress on bio-oil conversion into bio-fuels and raw chemicals: a review. J Chem Technol Biotechnol 2019;94:670–89. https://doi.org/10.1002/jctb.5758.
[13] Zhao Z, Situmorang YA, An P, Chaihad N, Wang J, Hao X, et al. Hydrogen production from catalytic steam reforming of bio-oils: A critical review. Chem Eng Technol 2020;43:625–40. https://doi.org/10.1002/ceat.201900487.
[14] Bimbela F, Chen D, Ruiz J, García L, Arauzo J. Ni/Al coprecipitated catalysts modified with magnesium and copper for the catalytic steam reforming of model compounds from biomass pyrolysis liquids. Appl Catal B Environ 2012;119–120:1–12. https://doi.org/10.1016/j.apcatb.2012.02.007.
[15] Bimbela F, Oliva M, Ruiz J, García L, Arauzo J. Hydrogen production via catalytic steam reforming of the aqueous fraction of bio-oil using nickel-based coprecipitated catalysts. Int J Hydrogen Energy 2013;38:14476–87. https://doi.org/10.1016/j.ijhydene.2013.09.038.
[16] Arandia A, Remiro A, García V, Castaño P, Bilbao J, Gayubo A. Oxidative steam reforming of raw bio-oil over supported and bulk Ni catalysts for hydrogen production. Catalysts 2018;8:322. https://doi.org/10.3390/catal8080322.
[17] Remiro A, Arandia A, Oar-Arteta L, Bilbao J, Gayubo AG. Regeneration of $NiAl_2O_4$ spinel type catalysts used in the reforming of raw bio-oil. Appl Catal B Environ 2018;237:353–65. https://doi.org/10.1016/j.apcatb.2018.06.005.
[18] Arandia A, Remiro A, Valle B, Bilbao J, Gayubo AG. Deactivation of Ni spinel derived catalyst during the oxidative steam reforming of raw bio-oil. Fuel 2020;276. https://doi.org/10.1016/j.fuel.2020.117995.
[19] García-Gómez N, Valecillos J, Remiro A, Valle B, Bilbao J, Gayubo AG. Effect of reaction conditions on the deactivation by coke of a $NiAl_2O_4$ spinel derived catalyst in the steam reforming of bio-oil. Appl Catal B Environ 2021;297:120445. https://doi.org/10.1016/j.apcatb.2021.120445.
[20] Valecillos J, Iglesias-Vázquez S, Landa L, Remiro A, Bilbao J, Gayubo AG. Insights into the reaction routes for H_2 formation in the ethanol steam reforming on a catalyst rerived from $NiAl_2O_4$ spinel. Energy Fuels 2021;35:17197–211. https://doi.org/10.1021/acs.energyfuels.1c01670.
[21] Bimbela F, Ábrego J, Puerta R, García L, Arauzo J. Catalytic steam reforming of the aqueous fraction of bio-oil using Ni-Ce/Mg-Al catalysts. Appl Catal B Environ 2017;209:346–57. https://doi.org/10.1016/j.apcatb.2017.03.009.
[22] Remón J, Medrano JA, Bimbela F, García L, Arauzo J. Ni/Al-Mg-O solids modified with Co or Cu for the catalytic steam reforming of bio-oil. Appl Catal B Environ 2013;132–133:433–44. https://doi.org/10.1016/j.apcatb.2012.12.015.
[23] Montero C, Oar-Arteta L, Remiro A, Arandia A, Bilbao J, Gayubo AG. Thermodynamic comparison between bio-oil and ethanol steam reforming. Int J Hydrogen Energy 2015;40:15963–71. https://doi.org/10.1016/j.ijhydene.2015.09.125.
[24] Rodrigues CT, Alonso CG, Machado GD, de Souza TL. Optimization of bio-oil steam reforming process by thermodynamic analysis. Int J Hydrogen Energy 2020;45:28350–60. https://doi.org/10.1016/j.ijhydene.2020.07.206.
[25] Landa L, Remiro A, De TR, Aguado R, Bilbao J, Gayubo G. Global vision from the thermodynamics of the effect of the bio-oil composition and the reforming strategies in the H_2 production and the energy requirement. Energy Convers Manag 2021;239:114181. https://doi.org/10.1016/j.enconman.2021.114181.
[26] Chen G, Yao J, Liu J, Yan B, Shan R. Biomass to hydrogen-rich syngas via catalytic steam reforming of bio-oil. Renew Energy 2016;91:315–22. https://doi.org/10.1016/j.renene.2016.01.073.
[27] Quan C, Xu S, Zhou C. Steam reforming of bio-oil from coconut shell pyrolysis over Fe/olivine catalyst. Energy Convers Manag 2017;141:40–7. https://doi.org/10.1016/j.enconman.2016.04.024.
[28] Valle B, Aramburu B, Olazar M, Bilbao J, Gayubo AG. Steam reforming of raw bio-oil over Ni/La2O3-AAl2O3: Influence of temperature on product yields and catalyst deactivation. Fuel 2018;216:463–74. https://doi.org/10.1016/j.fuel.2017.11.149.
[29] Valle B, Aramburu B, Benito PL, Bilbao J, Gayubo AG. Biomass to hydrogen-rich gas via steam reforming of raw bio-oil over Ni/La_2O_3-αAl_2O_3 catalyst: Effect of space-time and steam-to-carbon ratio. Fuel 2018;216:445–55. https://doi.org/10.1016/j.fuel.2017.11.151.
[30] Arregi A, Lopez G, Amutio M, Artetxe M, Barbarias I, Bilbao J, et al. Role of operating conditions in the catalyst deactivation in the in-line steam reforming of volatiles from biomass fast pyrolysis. Fuel 2018;216:233–44. https://doi.org/10.1016/j.fuel.2017.12.002.
[31] Arandia A, Remiro A, Oar-Arteta L, Bilbao J, Gayubo AG. Reaction conditions effect and pathways in the oxidative steam reforming of raw bio-oil on a Rh/CeO_2-ZrO_2 catalyst in a fluidized bed reactor. Int J Hydrogen Energy 2017;42:29175–85. https://doi.org/10.1016/j.ijhydene.2017.10.095.
[32] Remiro A, Arandia A, Oar-Arteta L, Bilbao J, Gayubo AG. Stability of a Rh/CeO_2-ZrO_2 catalyst in the oxidative steam reforming of raw bio-oil. Energy Fuels 2018;32:3588–98. https://doi.org/10.1021/acs.energyfuels.7b04141.
[33] Snoeck JW, Froment GF, Fowles M. Steam/CO_2 reforming of methane. Carbon filament formation by the Boudouard reaction and gasification by CO_2, by H_2, and by steam: Kinetic study. Ind Eng Chem Res 2002;41:4252–65. https://doi.org/10.1021/ie010666h.
[34] Koo KY, Lee SH, Jung UH, Roh HS, Yoon WL. Syngas production via combined steam and carbon dioxide reforming of methane over Ni-Ce/$MgAl_2O_4$ catalysts

with enhanced coke resistance. Fuel Process Technol 2014;119:151–7. https://doi.org/10.1016/j.fuproc.2013.11.005.
[35] He L, Hu S, Yin X, Xu J, Han H, Li H, et al. Promoting effects of Fe-Ni alloy on co-production of H_2 and carbon nanotubes during steam reforming of biomass tar over Ni-Fe/α-Al_2O_3. Fuel 2020;276:118116. https://doi.org/10.1016/j.fuel.2020.118116.
[36] Sehested J, Gelten JAP, Helveg S. Sintering of nickel catalysts: Effects of time, atmosphere, temperature, nickel-carrier interactions, and dopants. Appl Catal A Gen 2006;309:237–46. https://doi.org/10.1016/j.apcata.2006.05.017.
[37] Nabgan B, Nabgan W, Tuan Abdullah TA, Tahir M, Gambo Y, Ibrahim M, et al. Parametric study on the steam reforming of phenol-PET solution to hydrogen production over Ni promoted on Al_2O_3-La_2O_3catalyst. Energy Convers Manag 2017;142:127–42. https://doi.org/10.1016/J.ENCONMAN.2017.03.046.
[38] Kumar A, Sinha ASK. Hydrogen production from acetic acid steam reforming over nickel-based catalyst synthesized via MOF process. Int J Hydrogen Energy 2020;45:24397–411. https://doi.org/10.1016/j.ijhydene.2020.06.040.
[39] Montero C, Remiro A, Benito PL, Bilbao J, Gayubo AG. Optimum operating conditions in ethanol steam reforming over a Ni/La_2O_3-αAl_2O_3 catalyst in a fluidized bed reactor. Fuel Process Technol 2018;169:207–16. https://doi.org/10.1016/j.fuproc.2017.10.003.
[40] Kechagiopoulos PN, Voutetakis SS, Lemonidou AA, Vasalos IA. Hydrogen production via reforming of the aqueous phase of bio-oil over Ni/olivine catalysts in a spouted bed reactor. Ind Eng Chem Res 2009;48:1400–8. https://doi.org/10.1021/ie8013378.
[41] Lan P, Xu Q, Zhou M, Lan L, Zhang S, Yan Y. Catalytic steam reforming of fast pyrolysis bio-oil in fixed bed and fluidized bed reactors. Chem Eng Technol 2010;33:2021–8. https://doi.org/10.1002/CEAT.201000169.
[42] Montero C, Remiro A, Valle B, Oar-Arteta L, Bilbao J, Gayubo AG. Origin and nature of coke in ethanol steam Reforming and Its Role in Deactivation of Ni/La_2O_3-αAl_2O_3 catalyst. Ind Eng Chem Res 2019;58:14736–51. https://doi.org/10.1021/acs.iecr.9b02880.
[43] Oar-Arteta L, Remiro A, Aguayo AT, Bilbao J, Gayubo AG. Effect of operating conditions on dimethyl ether steam reforming over a $CuFe_2O_4$/γ-Al_2O_3 bifunctional catalyst. Ind Eng Chem Res 2015;54:9722–32. https://doi.org/10.1021/acs.iecr.5b02368.
[44] Jia H, Zhang J, Yu J, Yang X, Sheng X, Xu H, et al. Efficient H_2 production via membrane-assisted ethanol steam reforming over Ir/CeO_2 catalyst. Int J Hydrogen Energy 2019;44:24733–45. https://doi.org/10.1016/J.IJHYDENE.2019.07.199.
[45] Ma Z, Xiao R, Zhang H. Catalytic steam reforming of bio-oil model compounds for hydrogen-rich gas production using bio-char as catalyst. Int J Hydrogen Energy 2017;42:3579–85. https://doi.org/10.1016/j.ijhydene.2016.11.107.
[46] Hu X, Lu G. Investigation of the effects of molecular structure on oxygenated hydrocarbon steam re-forming. Energy Fuels 2009;23:926–33. https://doi.org/10.1021/ef8008647.
[47] Li X, Zhang Z, Zhang L, Fan H, Li X, Liu Q, et al. Investigation of coking behaviors of model compounds in bio-oil during steam reforming. Fuel 2020;265:116961. https://doi.org/10.1016/j.fuel.2019.116961.
[48] Li X, Zhang L, Li Q, Zhang Z, Zhang S, Li Y, et al. Steam reforming of sugars: Roles of hydroxyl group and carbonyl group in coke formation. Fuel 2021;292:120282. https://doi.org/10.1016/j.fuel.2021.120282.
[49] Li X, Zhang L, Zhang S, Xu L, Hu X. Steam reforming of sugar and its derivatives: Functionality dictates thermal properties and morphologies of coke. Fuel 2022;307:121798. https://doi.org/10.1016/j.fuel.2021.121798.
[50] Zhang Z, Sun Y, Wang Y, Sun K, Gao Z, Xu Q, et al. Steam reforming of acetic acid and guaiacol over Ni/Attapulgite catalyst: Tailoring pore structure of the catalyst with KOH activation for enhancing the resistivity towards coking. Mol Catal 2020;493. https://doi.org/10.1016/j.mcat.2020.111051.
[51] Remón J, Broust F, Volle G, García L, Arauzo J. Hydrogen production from pine and poplar bio-oils by catalytic steam reforming. Influence of the bio-oil composition on the process. Int J Hydrogen Energy 2015;40:5593–608. https://doi.org/10.1016/J.IJHYDENE.2015.02.117.
[52] Valle B, García-Gómez N, Arandia A, Remiro A, Bilbao J, Gayubo AG. Effect of phenols extraction on the behavior of Ni-spinel derived catalyst for raw bio-oil steam reforming. Int J Hydrogen Energy 2019;44:12593–603. https://doi.org/10.1016/j.ijhydene.2018.12.057.
[53] García-Gómez N, Valle B, Valecillos J, Remiro A, Bilbao J, Gayubo AG. Feasibility of online pre-reforming step with dolomite for improving Ni spinel catalyst stability in the steam reforming of raw bio-oil. Fuel Process Technol 2021;215:106769. https://doi.org/10.1016/j.fuproc.2021.106769.
[54] Ochoa A, Bilbao J, Gayubo AG, Castaño P. Coke formation and deactivation during catalytic reforming of biomass and waste pyrolysis products: A review. Renew Sustain Energy Rev 2020;119:109600. https://doi.org/10.1016/j.rser.2019.109600.
[55] Wang Y, Sun K, Zhang S, Xu L, Hu G, Hu X. Steam reforming of alcohols and carboxylic acids: Importance of carboxyl and alcoholic hydroxyl groups on coke properties. J Energy Inst 2021;98:85–97. https://doi.org/10.1016/j.joei.2021.06.002.
[56] Ochoa A, Aramburu B, Valle B, Resasco DE, Bilbao J, Gayubo AG, et al. Role of oxygenates and effect of operating conditions in the deactivation of a Ni supported catalyst during the steam reforming of bio-oil. Green Chem 2017;19:4315–33. https://doi.org/10.1039/C7GC01432E.
[57] Remiro A, Valle B, Aguayo AT, Bilbao J, Gayubo AG. Steam reforming of raw bio-oil in a fluidized bed reactor with prior separation of pyrolytic lignin. Energy Fuels 2013;27:7549–59. https://doi.org/10.1021/ef401835s.
[58] Valle B, Aramburu B, Remiro A, Arandia A, Bilbao J, Gayubo AG. Optimal conditions of thermal treatment unit for the steam reforming of raw bio-oil in a continuous two-step reaction system. Chem Eng Trans 2017;57:205–10. https://doi.org/10.3303/CET1757035.
[59] Du J, Gao J, Gu F, Zhuang J, Lu B, Jia L, et al. A strategy to regenerate coked and sintered Ni/Al2O3 catalyst for methanation reaction. Int J Hydrogen Energy 2018;43:20661–70. https://doi.org/10.1016/j.ijhydene.2018.09.128.
[60] Hasan M, Drazin J, Dey S, Castro RHR. Synthesis of stoichiometric nickel aluminate spinel nanoparticles. Am Mineral 2015;100:652–7. https://doi.org/10.2138/am-2015-4997.
[61] Valle B, García-Gómez N, Remiro A, Bilbao J, Gayubo AG. Dual catalyst-sorbent role of dolomite in the steam reforming of raw bio-oil for producing H_2-rich syngas. Fuel Process Technol 2020;200. https://doi.org/10.1016/j.fuproc.2019.106316.
[62] Han Y, Pinheiro Pires AP, Denson M, McDonald AG, Garcia-Perez M. Ternary phase diagram of water/bio-oil/organic solvent for bio-oil fractionation. Energy Fuels 2020;34:16250–64. https://doi.org/10.1021/acs.energyfuels.0c03100.
[63] Montero C, Ochoa A, Castaño P, Bilbao J, Gayubo AG. Monitoring Ni^0 and coke evolution during the deactivation of a Ni/La_2O_3-αAl_2O_3 catalyst in ethanol steam reforming in a fluidized bed. J Catal 2015;331:181–92. https://doi.org/10.1016/j.jcat.2015.08.005.
[64] Schuepfer DB, Badaczewski F, Guerra-Castro JM, Hofmann DM, Heiliger C, Smarsly B, et al. Assessing the structural properties of graphitic and non-graphitic carbons by Raman spectroscopy. Carbon N Y 2020;161:359–72. https://doi.org/10.1016/j.carbon.2019.12.094.
[65] Ferrari AC, Robertson J. Interpretation of Raman spectra of disordered and amorphous carbon. Phys Rev B 2000;61:14095–107. https://doi.org/10.1103/PhysRevB.61.14095.
[66] Chen K, Zhang H, Ibrahim UK, Xue WY, Liu H, Guo A. The quantitative assessment of coke morphology based on the Raman spectroscopic characterization of serial petroleum cokes. Fuel 2019;246:60–8. https://doi.org/10.1016/j.fuel.2019.02.096.
[67] He L, Hu S, Jiang L, Liao G, Zhang L, Han H, et al. Co-production of hydrogen and carbon nanotubes from the decomposition/reforming of biomass-derived organics over Ni/α-Al_2O_3 catalyst: Performance of different compounds. Fuel 2017;210:307–14. https://doi.org/10.1016/j.fuel.2017.08.080.
[68] Landa L, Remiro A, Valecillos J, Valle B, Bilbao J, Gayubo AG. Unveiling the deactivation by coke of $NiAl_2O_4$ spinel derived catalysts in the bio-oil steam reforming: Role of individual oxygenates. Fuel 2022;321:124009. https://doi.org/10.1016/j.fuel.2022.124009.
[69] He L, Liao G, Li H, Ren Q, Hu S, Han H, et al. Evolution characteristics of different types of coke deposition during catalytic removal of biomass tar. J Energy Inst 2020;93:2497–504. https://doi.org/10.1016/j.joei.2020.08.009.
[70] Gayubo AG, Aguayo AT, Atutxa A, Aguado R, Olazar M, Bilbao J. Transformation of oxygenate components of biomass pyrolysis oil on a HZSM-5 zeolite. II. Aldehydes, ketones, and acids. Ind Eng Chem Res 2004;43:2619–26. https://doi.org/10.1021/ie030792g.